

Cosmic microwave background spectral distortions from Rayleigh scattering at second order

Atsuhisa Ota^{1*}

¹*HKUST Jockey club Institute for Advanced Study,*

The Hong Kong University of Science and Technology, Clearwater Bay, Hong Kong, P.R.China

(Dated: April 19, 2022)

Cosmic microwave background (CMB) spectral distortion from Rayleigh scattering is calculated for the first time in rigorous second-order cosmological perturbation theory. The new spectral distortion is sensitive to acoustic dissipation at $10^{-2} < k\text{Mpc}/h < 1$, which slightly extends the scale constrained by the CMB anisotropies. The spectral shape is different from either temperature perturbations or any other traditional spectral distortions from Compton scattering, such as y and μ . The new spectral distortion is not formed in the late Universe, unlike the thermal Sunyaev-Zel'dovich effect degenerated with the primordial y distortions since photons must be hot for Rayleigh scattering. Therefore, ideal measurements can distinguish the signal from the other effects and extract new information during recombination. Assuming cosmological parameters consistent with the recent CMB anisotropy measurements, we find the new spectral distortion is $6.5 \times 10^{-3} \text{Jy/str}$, which is one order of magnitude smaller than the currently proposed target sensitivity range of voyage 2050.

I. INTRODUCTION

Spectral distortions of the cosmic microwave background (CMB) are potential cosmological observables for the next decades [1–3]. Although cosmologists have prioritized the anisotropy measurements to spectrum measurements since COBE FIRAS reported the almost ideal black body spectrum in 1996 [4], several observational projects are envisioned or ongoing targeting tiny spectral distortions [5–7], including extreme measurements proposed for voyage 2050 [8, 9]. The spectral distortions are formed due to various non-equilibrium phenomena in the Universe. For example, acoustic dissipation of short-scale cosmological perturbations [10–15], atomic processes during recombination [16–19], and energy injection from unknown sectors [20–27] can introduce the distortions. There is no universal prescription for non-equilibrium physics, so considering all possible spectral distortions and their cosmological implications in depth must be indispensable.

Photons interact with free electrons via Thomson scattering during recombination. While we normally ignore electrons bounded in atoms, those are also scattered, which is known as Rayleigh scattering. Rayleigh scattering is also elastic as Thomson scattering, but the cross-section is frequency-dependent. This is because the bounded electrons are more likely to interact with photons whose energy is close to the energy gaps $h\nu_i$ of the electron states. The Rayleigh cross section is Taylor-expanded and behaves as $(\nu/\nu_i)^4$ during recombination.

Ref. [28] showed that Rayleigh scattering of neutral hydrogen induces additional scattering, which changes the damping scale in the CMB anisotropies. Ref. [29] included neutral helium and polarization, and they presented a precise numerical calculation of the CMB an-

gular power spectrum. Then, Ref. [30] developed a moment expansion for the frequency dependence and estimated the back reaction of Rayleigh scattering to baryon acoustic oscillation. Recently, the Rayleigh anisotropies are also considered for constraining primordial non-Gaussianity and neutrino mass in Refs. [31, 32]. Thus, previous works on Rayleigh scattering are about the linear anisotropies.

While the photon spectrum is considered to be a local Planck in the early Universe, a spectral distortion is secondarily sourced by Silk damping of small-scale anisotropies [11, 33–37]. Physically speaking, acoustic oscillation of the viscous fluid leads to friction heat at second order, and the energy release distorts the fiducial Planck spectrum when the Universe is out of chemical equilibrium. Including Rayleigh scattering, the acoustic source can also be frequency-dependent, and then Rayleigh scattering at second order will introduce a different spectral distortion. This paper computes the spectral distortion generated by second-order Rayleigh scattering for the first time. Based on a rigorous framework of the general relativistic Boltzmann equation, we compute the spectral distortion due to Rayleigh scattering and discuss the size, detectability, and ability to constrain cosmological models.

We organize the paper as follows. In section II, we provide the Rayleigh scattering cross-section for neutral hydrogen, helium, and singly ionized helium numerically. Then we review the first-order Rayleigh anisotropies in section III. Section IV is the main part of the paper. We derive the spectral distortion from Rayleigh scattering at second order. We discuss several possible cosmological constraints on the new spectral distortions in Section V. Finally, we conclude the paper in Section VI.

* iasota@ust.hk

TABLE I. Expansion factors for Rayleigh scattering. The neutral hydrogen and the neutral helium parameters are taken from Ref. [30], and singly ionized helium is obtained as $c_{2i+4}^{(\text{HeII})} = c_{2i+4}^{(\text{H})}/2^{8+4i}$ as discussed in Ref. [38].

$2i+4$	$c_{2i+4}^{(\text{HI})}$	$c_{2i+4}^{(\text{HeI})}$	$c_{2i+4}^{(\text{HeII})}$
4	1.265625	0.120798	0.00494385
6	3.738281	0.067243	0.000912666
8	8.813931	0.031585	0.00013449
10	19.153795	0.014153	0.0000182665
12	39.923032	0.006226	2.3796×10^{-6}

II. SCATTERING CROSS SECTION

During recombination, singly ionized helium (HeII) is first produced and then neutral helium (HeI) is formed. In the last stage of recombination, the remaining electrons are captured in neutral hydrogen (HI) atoms. Rayleigh scattering starts after singly ionized helium appears at $z \sim 6000$. The non-relativistic Rayleigh scattering cross section including those three species is expanded into [30]

$$\sigma_R = \sigma_T \sum_{j=\text{HI,HeI,HeII}} \sum_{i=0}^{\infty} c_{2i+4}^{(j)} \Lambda^{2i+4} x^{2i+4}, \quad (1)$$

where σ_T is the Thomson scattering cross section, and we introduced

$$x \equiv \frac{h\nu}{k_B T_{\text{CMB}}} = 0.0176119 \left(\frac{\nu}{\text{GHz}} \right), \quad (2)$$

$$\Lambda \equiv \frac{k_B T_{\text{CMB}}}{a \text{Ry}} = \frac{1.72663}{a} \times 10^{-5}, \quad (3)$$

with the Rydberg constant Ry, the Boltzmann constant k_B , the present CMB temperature T_{CMB} , the Planck constant h , the comoving frequency ν , and the scale factor a . $c_{2i+4}^{(j)}$ are summarized in Tab. I. The expansion parameters for HI and HeI are taken from Tab.1 of Ref. [30]. As discussed in Ref. [38], the Rayleigh scattering cross-section for hydrogen-like atoms of atomic number Z is given as $c_{2i+4}^{(\text{HI})}/Z^{8+4i}$, and we consider HeII as a hydrogen-like atom of atomic number $Z = 2$. The differential optical depth is expanded as

$$\dot{\tau} = \dot{\tau}^{(0)} + x^4 \dot{\tau}^{(4)} + x^6 \dot{\tau}^{(6)} + x^8 \dot{\tau}^{(8)} + \dots, \quad (4)$$

where $\dot{\tau}^{(0)} = -n_e \sigma_T a$ with the free electron number density n_e and

$$\dot{\tau}^{(2i+4)} = \dot{\tau}^{(0)} \sum_{j=\text{HI,HeI,HeII}} \frac{n_j}{n_e} c_{2i+4}^{(j)} \Lambda^{2i+4}. \quad (5)$$

n_j is the number density of j . We find the number density of ions by modifying a recombination code **RECFAST** [39]. By default, **RECFAST** provides hydrogen ionization fraction $x_{\text{H}0}$, helium ionization fraction $x_{\text{He}0}$, electron ionization fraction x_e , and helium mass fraction f_{He} . Using

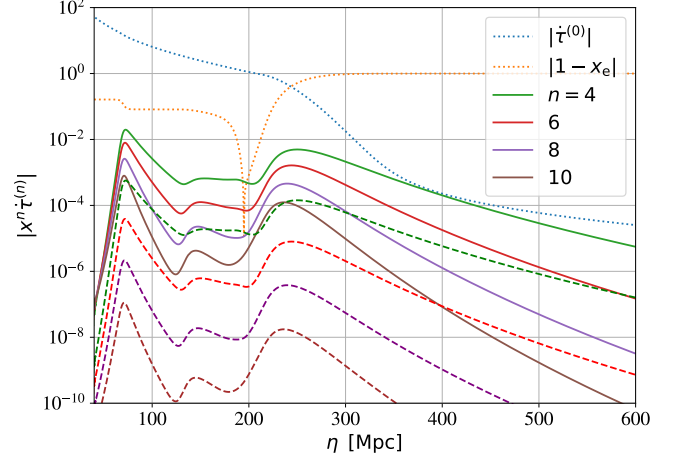


FIG. 1. The differential optical depth multiplied by x^n for various frequencies. The solid and dashed curves imply 857GHz and 357GHz, respectively. The peak at $\eta \lesssim 100\text{Mpc}$ is Rayleigh scattering of the singly ionized helium, which is bigger than the peak of neutral hydrogen.

those parameters, we get

$$\frac{n_{\text{HI}}}{n_e} = x_e^{-1} (1 - x_{\text{H}0}), \quad (6)$$

$$\frac{n_{\text{HeI}}}{n_e} = x_e^{-1} f_{\text{He}} (1 - x_{\text{He}0}), \quad (7)$$

where n_{H} and n_{He} are the total number densities of hydrogen and helium. Moreover, eliminating the number density of doubly ionized helium n_{HeIII} from

$$x_{\text{He}0} = \frac{n_{\text{HeII}}}{n_{\text{He}}} + \frac{n_{\text{HeIII}}}{n_{\text{He}}}, \quad (8)$$

$$x_e = 1 - \frac{n_{\text{HI}}}{n_{\text{H}}} + \frac{n_{\text{HeII}}}{n_{\text{H}}} + 2 \frac{n_{\text{HeIII}}}{n_{\text{H}}}, \quad (9)$$

we find

$$\frac{n_{\text{HeII}}}{n_e} = x_e^{-1} x_{\text{H}0} + 2 x_e^{-1} f_{\text{He}} x_{\text{He}0} - 1. \quad (10)$$

With Eqs. (5), (6) and (7), we reproduced the Rayleigh scattering differential optical depth in Refs. [29] and [30] for $\eta > 100\text{Mpc}$, and we can see a new feature in $\eta < 100\text{Mpc}$ in our Fig 1 with Eq. (10). While the number fraction of HeII is smaller than HI, the differential optical depth is comparable to HI because photons are hotter at higher redshift. Integrating the differential optical depth at 875GHz, we find $\tau^{(4)} x^4 \sim 0.8$, i.e., 80% of photons scatter on $\eta < 50\text{Mpc}$. This fact implies that Rayleigh scattering at $\eta < 50\text{Mpc}$ might be important for small scale. While we mainly use **RECFAST** in our calculation, we also reproduced Fig. 1 using another efficient modern numerical recombination code **HyRec** [40]. We crosschecked the new effect of singly ionized helium Rayleigh scattering.

III. RAYLEIGH SCATTERING AT FIRST ORDER

We have reviewed background thermodynamics in the previous section. Now we are ready to compute the evolution of the linear Rayleigh anisotropies.

A. Boltzmann equation

We will solve the Boltzmann equation for the photon phase-space distribution function (PDF) in the presence of Thomson and Rayleigh scattering with other cosmological matter contents and the Einstein equation. It is quite difficult to solve the nonlinear partial differential equations in a general setup, so we perturbatively solve the equation order by order on top of a homogenous and isotropic Friedman background.

The Universe is in local chemical equilibrium in the early epoch, but photon production processes decouple as the Universe expands. The blackbody photosphere is around the redshift 2×10^6 when double Compton scattering becomes inefficient. Thomson scattering and its relativistic correction are dominant afterward until the end of recombination. The photon fluid is defused due to the scattering, and deviation from the Planck distribution is introduced. Therefore, the solution to the photon Boltzmann equation should be written as a local Planck distribution with small spectral distortions. Indeed, we immediately find the background solution is a homogeneous and isotropic Planck distribution (See, e.g., [41])

$$f_{\text{pl}}(x) \equiv \frac{1}{e^x - 1}, \quad (11)$$

with x defined in Eq. (2). We perturb the Planck distribution as $f = f_{\text{pl}}(xe^{-\Theta})$ or equivalently T_{CMB} as $T_{\text{CMB}}e^{\Theta}$, with the temperature perturbation Θ . Taylor expanding $f_{\text{pl}}(xe^{-\Theta})$ with respect to Θ up to first order, we find

$$f_{\text{pl}}(xe^{-\Theta}) = f_{\text{pl}}(x) + \Theta \mathcal{G}^{(0)}(x) + \mathcal{O}(\Theta^2), \quad (12)$$

where we defined

$$\mathcal{G}^{(0)}(x) \equiv -x \frac{\partial}{\partial x} f_{\text{pl}}(x). \quad (13)$$

Θ is frequency independent and is a function of photon momentum direction \mathbf{n} , position \mathbf{x} and conformal time η , for Thomson scattering. $\mathcal{G}^{(0)}$ is the frequency shape of the first order temperature shift. Rayleigh scattering shifts the spectrum by x^{2n+4} . Hence, the temperature perturbation for Rayleigh scattering carries additional powers of x . The linearized spectrum including Rayleigh scattering can be parameterized by [30]

$$f = f_{\text{pl}} + \mathcal{G}^{(0)}\Theta^{(0)} + \mathcal{G}^{(4)}\Theta^{(4)} + \dots, \quad (14)$$

where we include the power of x into

$$\mathcal{G}^{(n)} \equiv x^n \mathcal{G}^{(0)}. \quad (15)$$

The dots imply the Rayleigh scattering corrections of $x^{n>4}$. Rayleigh scattering happens at most 1/10 times during cosmic history for the major frequencies so that the frequency cascade typically happens just once per photon, and the Rayleigh scattered photons are mostly Thomson scattered during the rest of cosmic history. Therefore, hereafter we truncate series expansions for x at this order unless otherwise stated. Since $\mathcal{G}^{(4)}$ perfectly characterizes the frequency dependence at this order, we do not have to consider many samples in the frequency space for calculations [30]. The Liouville term up to first order in the cosmological perturbation is written as

$$\mathcal{L}[f] = \left(\Theta^{(0)'} - (\ln x)' \right) \mathcal{G}^{(0)} + \mathcal{G}^{(4)} \Theta^{(4)'}. \quad (16)$$

A prime is an ordinary derivative with respect to conformal time. The time derivatives of functions of x are higher-order perturbations as $(\ln x)'$ is first order in metric perturbations [42]. The linear collision term for Thomson scattering is given as (See, e.g., [41])

$$\mathcal{C}[f] = \dot{\tau}^{(0)} \left(f - f_0 + x \frac{\partial f}{\partial x} V + \frac{1}{2} f_2 P_2 \right), \quad (17)$$

where $V \equiv \mathbf{v} \cdot \mathbf{n}$ with the baryon bulk velocity \mathbf{v} , the Legendre polynomial P_ℓ of the cosine between \mathbf{n} and \mathbf{v} , and the multiple coefficient f_ℓ . Following Refs. [28, 29] we obtain the linear Rayleigh collision term by replacing $\dot{\tau}^{(0)}$ in Eq. (17) with Eq. (4). Substituting Eqs. (14) and (4) into (17), we find

$$\mathcal{C}[f] = \dot{\tau}^{(0)} \mathcal{A}^{(0)} \mathcal{G}^{(0)} + \dot{\tau}^{(0)} \mathcal{A}^{(4)} \mathcal{G}^{(4)} + \dot{\tau}^{(4)} \mathcal{A}^{(0)} \mathcal{G}^{(4)}, \quad (18)$$

where we introduced

$$\mathcal{A}^{(n)} \equiv \Theta^{(n)} - \Theta_0^{(n)} - \delta_{n0} V + \frac{1}{2} \Pi^{(n)} P_2, \quad (19)$$

$$\mathcal{A}_{\text{P}}^{(n)} \equiv \Theta_{\text{P}}^{(n)} - \frac{1}{2} \Pi^{(n)} (1 - P_2). \quad (20)$$

We included polarization by replacing Θ_2 with $\Pi \equiv \Theta_2 + \Theta_{\text{P}0} + \Theta_{\text{P}2}$. Θ_{P} is polarization temperature perturbation, which corresponds to $G_\gamma = 4\Theta_{\text{P}}$ in Ref. [42].

From Eqs. (18) and (16), the linear order part of the Boltzmann equation $\mathcal{L}[f] = \mathcal{C}[f]$ can be obtained as

$$\Theta^{(0)'} - (\ln x)' = \dot{\tau}^{(0)} \mathcal{A}^{(0)}, \quad (21)$$

$$\Theta^{(4)'} = \dot{\tau}^{(0)} \mathcal{A}^{(4)} + \dot{\tau}^{(4)} \mathcal{A}^{(0)}. \quad (22)$$

The first equation is the standard Thomson scattering Boltzmann equation. The second equation is the first moment of Rayleigh scattering proportional to $\mathcal{G}^{(4)}$. The gravitational redshift $(\ln x)'$ does not introduce the Rayleigh anisotropies. The above derivation straightforwardly applies to the linear Rayleigh polarization.

B. Boltzmann Hierarchy equations

Linear scalar perturbations associated with the photon PDF are decomposed into

$$\Theta^{(n)} = (4\pi) \sum_{\ell m} i^\ell \int_{\mathbf{k}} e^{i\mathbf{k}\cdot\mathbf{x}} Y_{\ell m}^*(\hat{k}) Y_{\ell m}(\mathbf{n}) \tilde{\Theta}_\ell^{(n)} \zeta_{\mathbf{k}}, \quad (23)$$

$$V = (4\pi) \sum_m i \int_{\mathbf{k}} e^{i\mathbf{k}\cdot\mathbf{x}} Y_{1m}^*(\hat{k}) Y_{1m}(\mathbf{n}) \tilde{V}_1 \zeta_{\mathbf{k}}, \quad (24)$$

where a tilde implies the transfer function in Fourier space, $\int_{\mathbf{k}} \equiv \int (2\pi)^{-3} d^3k$ and $\zeta_{\mathbf{k}}$ is the initial Gaussian stochastic variable that satisfies

$$\langle \zeta_{\mathbf{k}} \zeta_{\mathbf{k}'} \rangle = (2\pi)^3 \delta_{\mathbf{D}}^{(3)}(\mathbf{k} + \mathbf{k}') \frac{2\pi^2}{k^3} \mathcal{P}_\zeta(k). \quad (25)$$

\mathcal{P}_ζ contains the details of inflationary cosmology. Expanding the above equations into the Legendre coefficients, we get the Boltzmann hierarchy equations for Rayleigh scattering [29, 30]

$$\dot{\tilde{\Theta}}_0^{(4)} = -k \tilde{\Theta}_1^{(4)}, \quad (26)$$

$$\dot{\tilde{\Theta}}_1^{(4)} = \dot{\tau}^{(0)} \tilde{\Theta}_1^{(4)} + \frac{k}{3} \left(\tilde{\Theta}_0^{(4)} - 2\tilde{\Theta}_2^{(4)} \right) + \dot{\tau}^{(4)} \tilde{\Theta}_{1g}^{(0)}, \quad (27)$$

$$\dot{\tilde{\Theta}}_2^{(4)} = \frac{k}{5} \left(2\tilde{\Theta}_1^{(4)} - 3\tilde{\Theta}_3^{(4)} \right) + \dot{\tau}^{(4)} \left(\tilde{\Theta}_2^{(0)} - \frac{\tilde{\Pi}^{(0)}}{10} \right) + \dot{\tau}^{(0)} \left(\tilde{\Theta}_2^{(4)} - \frac{\tilde{\Pi}^{(4)}}{10} \right), \quad (28)$$

$$\dot{\tilde{\Theta}}_{\ell \geq 3}^{(4)} = \frac{k}{2\ell + 1} \left(\ell \tilde{\Theta}_{\ell-1}^{(4)} - (\ell + 1) \tilde{\Theta}_{\ell+1}^{(4)} \right) + \dot{\tau}^{(4)} \tilde{\Theta}_\ell^{(0)} + \dot{\tau}^{(0)} \tilde{\Theta}_\ell^{(4)}, \quad (29)$$

where we introduce the photon-baryon velocity difference $\tilde{\Theta}_{1g}^{(0)} \equiv \tilde{\Theta}_1^{(0)} - \tilde{V}_1$. The polarization hierarchy equations are [29, 30]

$$\dot{\tilde{\Theta}}_{P,0}^{(4)} = -k \tilde{\Theta}_{P,1}^{(4)} + \dot{\tau}^{(0)} \left(\tilde{\Theta}_{P0}^{(4)} - \frac{\tilde{\Pi}^{(4)}}{2} \right) + \dot{\tau}^{(4)} \left(\tilde{\Theta}_{P0}^{(0)} - \frac{\tilde{\Pi}^{(0)}}{2} \right), \quad (30)$$

$$\dot{\tilde{\Theta}}_{P,1}^{(4)} = \dot{\tau}^{(0)} \tilde{\Theta}_{P,1}^{(4)} + \frac{k}{3} \left(\tilde{\Theta}_{P,0}^{(4)} - 2\tilde{\Theta}_{P,2}^{(4)} \right) + \dot{\tau}^{(4)} \tilde{\Theta}_{P,1}^{(0)}, \quad (31)$$

$$\dot{\tilde{\Theta}}_{P,2}^{(4)} = \frac{k}{5} \left(2\tilde{\Theta}_{P,1}^{(4)} - 3\tilde{\Theta}_{P,3}^{(4)} \right) + \dot{\tau}^{(4)} \left(\tilde{\Theta}_{P,2}^{(0)} - \frac{\tilde{\Pi}^{(0)}}{10} \right) + \dot{\tau}^{(0)} \left(\tilde{\Theta}_{P,2}^{(4)} - \frac{\tilde{\Pi}^{(4)}}{10} \right), \quad (32)$$

$$\dot{\tilde{\Theta}}_{P,\ell \geq 3}^{(4)} = \frac{k}{2\ell + 1} \left(\ell \tilde{\Theta}_{P,\ell-1}^{(4)} - (\ell + 1) \tilde{\Theta}_{P,\ell+1}^{(4)} \right) + \dot{\tau}^{(4)} \tilde{\Theta}_{P,\ell}^{(0)} + \dot{\tau}^{(0)} \tilde{\Theta}_{P,\ell}^{(4)}. \quad (33)$$

The hierarchy equations for Thomson scattering are unchanged as Eq. (21) does not contain Rayleigh scattering. The Rayleigh anisotropies and polarization are sourced by $\tilde{\Theta}_{1g}^{(0)}$, $\tilde{\Theta}_{\ell \geq 2}^{(0)}$ and $\tilde{\Theta}_{P,\ell}^{(0)}$, which are non-vanishing only on sub-horizon scale and are linear gauge invariants. The Boltzmann hierarchy equations for Rayleigh scattering are independent of the metric perturbations. From the above two facts, the Rayleigh anisotropies are gauge independent, and we can use the above hierarchy equations in any gauge. We truncate the Boltzmann hierarchy with the traditional method in Ref. [42]. In this paper, we numerically evaluate the Boltzmann hierarchy by modifying a publicly available linear Boltzmann solver CLASS [43] with cosmological parameters in Ref. [44].

C. Tight-coupling approximation

The Thomson Boltzmann hierarchy is a stiff system as it contains $\dot{\tau}^{(0)} \tilde{\Theta}_{1g}^{(0)}$. Before last scattering, $\dot{\tau}^{(0)}$ is large, $\tilde{\Theta}_1$ and \tilde{V}_1 are the almost same size; therefore, we need extra precision for both $\tilde{\Theta}_1$ and \tilde{V}_1 to get sufficiently accurate $\dot{\tau}^{(0)} \tilde{\Theta}_{1g}^{(0)}$. For efficient calculations, we directly find the evolution of $\tilde{\Theta}_{1g}$ by subtracting the Euler equations for photons and baryons. The equation is expanded into a series of $1/\dot{\tau}^{(0)}$ and CLASS truncates the series expansion at second order in $1/\dot{\tau}^{(0)}$ [43]. The multipole of $\ell > 3$ is $\mathcal{O}(1/\dot{\tau}^{(0)3})$ and we drop them during the tight coupling approximation. This simplification significantly reduces the number of equations to solve.

The Rayleigh anisotropies are produced by $\tilde{\Theta}_{1g}^{(0)}$ and higher multipoles $\tilde{\Theta}_{\ell \geq 2}^{(0)}$. In contrast to the Thomson hierarchy, the Rayleigh hierarchy is at most $\mathcal{O}(1/\dot{\tau}^{(0)2})$. Up

to second order in tight-coupling approximation, we find

$$\tilde{\Theta}_1^{(4)} \approx -\frac{\dot{\tau}^{(4)}}{\dot{\tau}^{(0)}} \tilde{\Theta}_{1g}^{(0)}, \quad (34)$$

and for $\ell > 1$,

$$\tilde{\Theta}_\ell^{(4)} \approx -\frac{\dot{\tau}^{(4)}}{\dot{\tau}^{(0)}} \tilde{\Theta}_\ell^{(0)}. \quad (35)$$

Similarly, polarization satisfies

$$\tilde{\Theta}_{P,\ell}^{(4)} \approx -\frac{\dot{\tau}^{(4)}}{\dot{\tau}^{(0)}} \tilde{\Theta}_{P,\ell}^{(0)}. \quad (36)$$

For simplicity, we also consider

$$\tilde{\Theta}_0^{(4)} = -k\eta \tilde{\Theta}_1^{(4)}. \quad (37)$$

The expansion scheme for the tight-coupling approximation is nicely reviewed in Ref. [43], and we use the same method. After the tight coupling approximation, we fully evolve the Rayleigh Boltzmann hierarchy. Adding the new hierarchy equations in the Boltzmann code is straightforward.

D. Back reaction

Back reaction of Rayleigh scattering appears in the Einstein equation and Euler equation for baryons because those equations contain x integrals of the photon distribution function [30]. The photon density perturbation is given by

$$\begin{aligned} \delta_\gamma &= \frac{\int x^3 dx \mathcal{G}^{(0)} (\tilde{\Theta}_0^{(0)} + \tilde{\Theta}_0^{(4)} x^4 + \dots)}{\int x^3 dx f_{\text{pl}}} \\ &= 4 \left(\tilde{\Theta}_0^{(0)} + \frac{I_4}{I_0} \tilde{\Theta}_0^{(4)} + \dots \right), \end{aligned} \quad (38)$$

where we have defined

$$I_n \equiv \int dx x^{n+3} \mathcal{G}^{(0)} = \zeta(n+4) \Gamma(n+5). \quad (39)$$

Similarly, we get photon fluid velocity divergence θ_γ , photon shear σ_γ , the higher order multipoles $F_{\gamma\ell}$ as

$$\theta_\gamma = 3k \left(\tilde{\Theta}_1^{(0)} + \frac{I_4}{I_0} \tilde{\Theta}_1^{(4)} + \dots \right), \quad (40)$$

$$\sigma_\gamma = 2 \left(\tilde{\Theta}_2^{(0)} + \frac{I_4}{I_0} \tilde{\Theta}_2^{(4)} + \dots \right), \quad (41)$$

$$F_{\gamma,\ell} = 4 \left(\tilde{\Theta}_\ell^{(0)} + \frac{I_4}{I_0} \tilde{\Theta}_\ell^{(4)} + \dots \right). \quad (42)$$

We use the above quantities for the right hand side of the Einstein equation. The Euler equation for baryons contains the integrated collision term

$$\dot{\tau}^{(0)} (\tilde{\Theta}_1^{(0)} - \tilde{V}_1) = \frac{\int x^3 \left[\dot{\tau}^{(0)} (\tilde{\Theta}_1^{(0)} - \tilde{V}_1) \right] \mathcal{G}^{(0)} dx}{4 \int x^3 f_{\text{pl}} dx}. \quad (43)$$

Including Rayleigh scattering, we modify the Thomson optical depth and $\tilde{\Theta}_1^{(0)}$ and we get

$$\dot{\tau}^{(0)} \left(\tilde{\Theta}_1^{(0)} + \frac{I_4}{I_0} \tilde{\Theta}_1^{(4)} - \tilde{V}_1 \right) + \frac{I_4}{I_0} \dot{\tau}^{(4)} (\tilde{\Theta}_1^{(0)} - \tilde{V}_1). \quad (44)$$

The back reaction is typically the order of $\mathcal{O}(I_4/I_0 \cdot \dot{\tau}^{(4)}/\dot{\tau}^{(0)})$.

IV. RAYLEIGH SCATTERING AT SECOND ORDER

Next, we consider Rayleigh scattering at second order. To be more precise, we are interested in the spectral distortion of the average CMB spectrum, so we only consider the angular averaged part at second order.

A. Collision integral

The monopole component of the Thomson scattering collision term up to second order is given as (see e.g., [36] for a derivation)

$$\begin{aligned} \mathcal{C}_0[f] &= -\dot{\tau}^{(0)} \left[V \left(3 + x \frac{\partial}{\partial x} \right) f \right]_0 \\ &\quad - \dot{\tau}^{(0)} \left[V^2 \left(x^2 \frac{\partial^2}{\partial x^2} + 4x \frac{\partial}{\partial x} \right) f \right]_0, \end{aligned} \quad (45)$$

where the subscript 0 implies the average with respect to the photon direction \mathbf{n} . The rest of the second-order collision terms are dropped after the angular average. The second-order collision term includes the relativistic correction of the bulk motion, which introduces the isotropic spectral distortions at second order (the Doppler shift).

Since Thomson scattering is an elastic scattering of a photon and an electron, it must rigorously preserve the number of photons for any f . In general, the covariant derivative of the photon number flux N^μ is related to the collision term as (see, e.g., [45])

$$\nabla_\mu N^\mu = c_1 \int x^2 dx \mathcal{C}_0[f], \quad (46)$$

where c_1 is a numerical factor of the Jacobian for the perturbed spacetime. Eq. (45) implies $x^2 \mathcal{C}_0[f]$ reduces to a total derivative for any f and thus the number flux conservation is always satisfied.

Rayleigh scattering is also elastic and must conserve the number of photons. However, the straightforward replacement of the differential optical depth in Eq. (45) does not guarantee the number conservation. The prescription does not work at second order simply because we ignored the incoming photon frequency dependence of Rayleigh scattering [46]. The non-relativistic limit Rayleigh scattering does not exchange photon energy so that the energies of incoming and outgoing photons are

always the same, but this is not the case when including relativistic corrections.

Derivative operators with respect to x in the collision integral appear when integrating by parts, the Taylor expanded the delta function responsible for the energy conservation of the scattering process. To be more specific, Eq. (45) is obtained after integrating \bar{x} out from the following type of integrals [36]

$$\int d\bar{x} \dot{\tau}^{(0)} [f(\bar{x}, \mathbf{n}) - f(x, \mathbf{n})] x^n \frac{\partial^n}{\partial \bar{x}^n} \delta_D(\bar{x} - x). \quad (47)$$

To properly account for \bar{x} dependence of the Rayleigh scattering, we include the Rayleigh cross section by replacing the differential optical depth in Eq. (47) as

$$\dot{\tau}^{(0)} \rightarrow \dot{\tau}^{(0)} + \bar{x}^4 \dot{\tau}^{(4)} + \dots \quad (48)$$

With this prescription, substituting the first order solution (14) and Eq. (48) into the second order Thomson collision integral, Eq. (45) yields

$$\begin{aligned} C_0[f] = & -\dot{\tau}^{(0)} \left[V^2 - V\Theta^{(0)} \right]_0 \mathcal{Y}^{(0)} \\ & + \dot{\tau}^{(0)} \left[V\Theta^{(4)} \right]_0 \mathcal{Y}^{(4)} \\ & - \dot{\tau}^{(4)} \left[V^2 - V\Theta^{(0)} \right]_0 \mathcal{Y}^{(4)}, \end{aligned} \quad (49)$$

where we introduced

$$\mathcal{Y}^{(0)} \equiv \left(-x \frac{\partial}{\partial x} \right) \mathcal{G}^{(0)} - 3\mathcal{G}^{(0)}, \quad (50)$$

$$\mathcal{Y}^{(n)} \equiv x^n \mathcal{Y}^{(0)} - n\mathcal{G}^{(n)}. \quad (51)$$

Note that the second-order correction to f turns into third-order correction in Eq. (49). The first term proportional to $\mathcal{Y}^{(0)}$ is the source term for the standard y spectral distortion from Thomson scattering [11]. $\mathcal{Y}^{(4)}$ is the new spectral distortion. Both spectral distortions preserve the number of photons as we have

$$\int x^2 dx \mathcal{Y}^{(n)} = 0. \quad (52)$$

B. Liouville term

The first-order solution fixes the second-order collision term Eq. (49). Our next step is to find second-order Liouville equation consistent with Eq. (49). For Thomson scattering, second-order ansatz can be written as [11, 33–37]

$$f_{\text{pl}} \left(x e^{-\Theta^{(0)}} \right) + y^{(0)} \mathcal{Y}^{(0)}. \quad (53)$$

where we ignored μ spectral distortion since we only consider recombination epoch when μ is not produced. The first term is nonlinearly perturbed Planck distribution, and the second term is the y distortion that we cannot

include in the temperature. Eq. (53) will be generalized to

$$f_{\text{pl}} \left(x e^{-\Theta^{(0)} - x^4 \Theta^{(4)}} \right) + y^{(0)} \mathcal{Y}^{(0)} + y^{(4)} \mathcal{Y}^{(4)}. \quad (54)$$

Similar to Thomson scattering, $y^{(0)}$ and $y^{(4)}$ represent the spectral distortion that cannot be included in the frequency dependent temperature perturbation $\Theta^{(0)} + x^4 \Theta^{(4)} + \dots$. Expanding this equation up to second order, we find

$$\begin{aligned} f = & f_{\text{pl}} + \Theta^{(0)} \mathcal{G} + \Theta^{(4)} \mathcal{G}^{(4)} \\ & + \frac{3}{2} \Theta^{(0)2} \mathcal{G}^{(0)} + 3\Theta^{(0)} \Theta^{(4)} \mathcal{G}^{(4)} \\ & + \frac{1}{2} \Theta^{(0)2} \mathcal{Y}^{(0)} + \Theta^{(0)} \Theta^{(4)} \mathcal{Y}^{(4)} \\ & + y^{(0)} \mathcal{Y}^{(0)} + y^{(4)} \mathcal{Y}^{(4)}, \end{aligned} \quad (55)$$

where we redefine second-order temperature perturbations as $\Theta^{(4)} \rightarrow \Theta^{(4)} - 4y^{(4)}$ for notational simplicity. Taking the time derivative of Eq. (55), we find

$$\begin{aligned} f' = & \left(1 + 3\Theta^{(0)} \right) \left(\Theta^{(0)'} - (\ln x)' \right) \mathcal{G}^{(0)} \\ & + \left[\left(1 + 3\Theta^{(0)} \right) \Theta^{(4)'} + 3\Theta^{(4)} \left(\Theta^{(0)'} - (\ln x)' \right) \right] \mathcal{G}^{(4)} \\ & + [y^{(0)'} + \Theta^{(0)} \left(\Theta^{(0)'} - (\ln x)' \right)] \mathcal{Y}^{(0)} \\ & + [y^{(4)'} + \Theta^{(0)} \Theta^{(4)'} + \Theta^{(4)} \left(\Theta^{(0)'} - (\ln x)' \right)] \mathcal{Y}^{(4)}, \end{aligned} \quad (56)$$

where we used the chain rule:

$$\mathcal{G}^{(n)'} = -(\ln x)' \left(\mathcal{Y}^{(n)} + 3\mathcal{G}^{(n)} \right). \quad (57)$$

We do not have to consider $\mathcal{Y}^{(n)'} since this term turns into a third-order correction that we ignore.$

C. Boltzmann equation

Equating Eqs. (49) and (56), with the linear collision terms (21) and (22), we find

$$\Theta_0^{(0)'} = -3\dot{\tau}^{(0)} [\Theta^{(0)} \mathcal{A}^{(0)}]_0, \quad (58)$$

$$\begin{aligned} \Theta_0^{(4)'} = & -3\dot{\tau}^{(0)} [\Theta^{(0)} \mathcal{A}^{(4)}]_0 - 3\dot{\tau}^{(4)} [\Theta^{(0)} \mathcal{A}^{(0)}]_0 \\ & - 3\dot{\tau}^{(0)} [\Theta^{(4)} \mathcal{A}^{(0)}]_0, \end{aligned} \quad (59)$$

$$y_0^{(0)'} = -\dot{\tau}^{(0)} [\Theta^{(0)} \mathcal{A}^{(0)}]_0 - \dot{\tau}^{(0)} \left[V^2 - V\Theta^{(0)} \right]_0, \quad (60)$$

$$\begin{aligned} y_0^{(4)'} = & -\dot{\tau}^{(0)} [\Theta^{(4)} \mathcal{A}^{(0)}]_0 - \dot{\tau}^{(0)} [\Theta^{(0)} \mathcal{A}^{(4)}]_0 \\ & + \dot{\tau}^{(0)} \left[V\Theta^{(4)} \right]_0 - \dot{\tau}^{(4)} [\Theta^{(0)} \mathcal{A}^{(0)}]_0 \\ & - \dot{\tau}^{(4)} \left[V^2 - V\Theta^{(0)} \right]_0. \end{aligned} \quad (61)$$

The source terms for $y_0^{(0)}$ and $y_0^{(4)}$ are given as products of the linear scalar perturbations. The ensemble

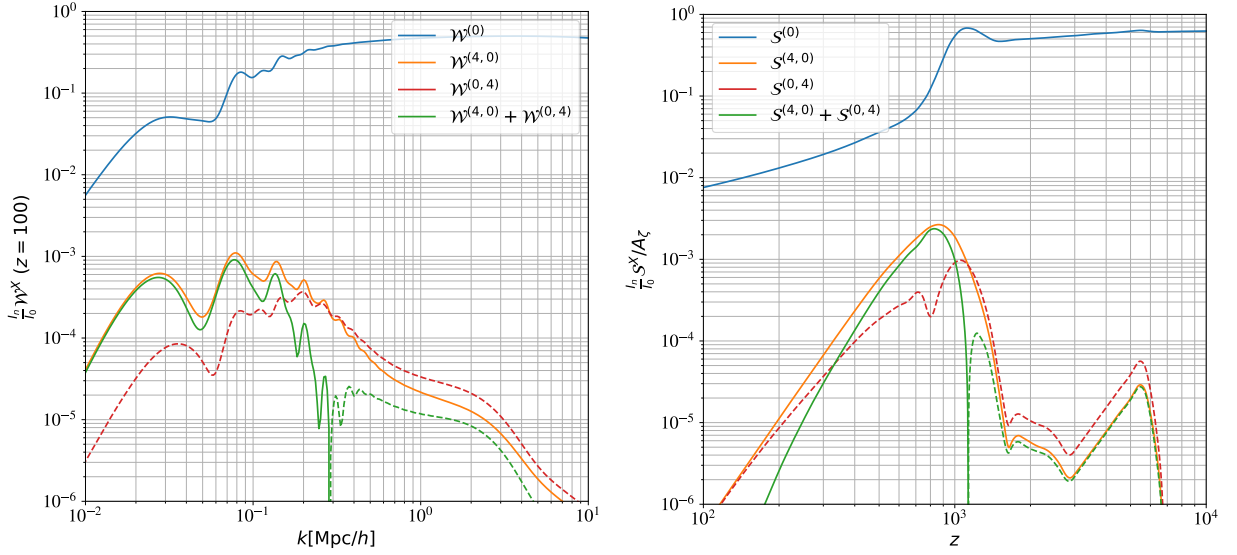


FIG. 2. *Left*: the Fourier space window function $I_n/I_0 \cdot \mathcal{W}^{(X)}$ for the spectral distortions at $z = 100$. The dashed curves imply the negative sign. $\mathcal{W}^{(0,4)} \approx -2\mathcal{W}^{(4,0)}$ so that the window function is negative during the tight coupling regime, but $\mathcal{W}^{(4,0)} > 0$ dominates after hydrogen recombination. *Right*: the spectral distortion source $I_n/I_0 \cdot \mathcal{S}^{(X)}$ for the primordial power spectrum of spectral index $n_s = 0.96$. Similarly, $\mathcal{S}^{(0,4)} \approx -2\mathcal{S}^{(4,0)}$ is established for high redshifts, but $\mathcal{S}^{(4,0)} > 0$ dominates after hydrogen recombination.

and angular average of a product of linear perturbations is evaluated as

$$\langle [AB]_0 \rangle = \int d \ln k \mathcal{P}_\zeta \sum_\ell (2\ell + 1) \tilde{A}_\ell \tilde{B}_\ell. \quad (62)$$

Using Eqs. (23), (24), (60), (61), and (62), we find

$$\langle y_0^{(0)} \rangle' = \int d \ln k \mathcal{P}_\zeta \mathcal{K}^{(0)}, \quad (63)$$

$$\langle y_0^{(4)} \rangle' = \int d \ln k \mathcal{P}_\zeta \left[\mathcal{K}^{(0,4)} + \mathcal{K}^{(4,0)} \right], \quad (64)$$

where we defined

$$-\frac{\mathcal{K}^{(0)}}{\dot{\tau}^{(0)}} = 3\tilde{\Theta}_{1g}^{(0)2} - \frac{\tilde{\Theta}_2^{(0)}\tilde{\Pi}^{(0)}}{2} + \sum_{\ell=2}^{\infty} (2\ell + 1) \tilde{\Theta}_\ell^{(0)2}, \quad (65)$$

$$-\frac{\mathcal{K}^{(0,4)}}{\dot{\tau}^{(0)}} = 6\tilde{\Theta}_1^{(4)}\tilde{\Theta}_{1g}^{(0)} - \frac{\tilde{\Theta}_2^{(4)}\tilde{\Pi}^{(0)}}{2} - \frac{\tilde{\Theta}_2^{(0)}\tilde{\Pi}^{(4)}}{2} + 2 \sum_{\ell=2}^{\infty} (2\ell + 1) \tilde{\Theta}_\ell^{(4)}\tilde{\Theta}_\ell^{(0)} \quad (66)$$

$$\mathcal{K}^{(4,0)} = \frac{\dot{\tau}^{(4)}}{\dot{\tau}^{(0)}} \mathcal{K}^{(0)}. \quad (67)$$

The gauge invariance of spectral distortions is critical as the spectral distortions are physical observables. The kernel function for the traditional y spectral distortion is composed of $\tilde{\Theta}_{1g}^{(0)}$ and $\tilde{\Theta}_{\ell \geq 2}^{(0)}$. Those variables are gauge invariant at linear order, so y distortion is also gauge invariant [11]. The new spectral distortion is sourced by $\tilde{\Theta}_{1g}^{(0)}$, $\tilde{\Theta}_{\ell \geq 2}^{(0)}$, and $\tilde{\Theta}_{\ell \geq 1}^{(4)}$. While $\tilde{\Theta}_1^{(0)}$ is gauge dependent,

$\tilde{\Theta}_1^{(4)}$ is not since it is sourced by $\tilde{\Theta}_{1g}^{(0)}$. Therefore, the new spectral distortion is also gauge invariant.

Energy release at high redshift is thermalized due to the energy transfer by high energy electrons. y and our new spectral distortions are realized when the thermalization effect is weak. Roughly speaking, the spectral dependence of the energy release after $z = 6 \times 10^4$ is not changed anymore, and Ref. [47] found a precise energy branching ratio

$$\mathcal{J}_y(z) = \frac{1}{1 + \left(\frac{1+z}{6.0 \times 10^4} \right)^{2.58}}, \quad (68)$$

and, $\mathcal{J}_y \mathcal{K}^{(X)}$ contributes to the new spectral distortion. Integrating Eq. (64) with respect to time, we finally get

$$\langle y_0^{(4)} \rangle = \int_{k_{\min}}^{k_{\max}} d \ln k \mathcal{P}_\zeta \left(\mathcal{W}^{(0,4)} + \mathcal{W}^{(4,0)} \right), \quad (69)$$

where we introduced the window function

$$\mathcal{W}^{(X)}(k, \eta) \equiv \int_0^\eta d\bar{\eta} \mathcal{J}_y \mathcal{K}^{(X)}. \quad (70)$$

The Fourier space window functions $\mathcal{W}^{(X)}$ are presented in the left panel of Fig. 2. In the figure, we normalized the window function by the energy fraction of the new spectral distortion

$$\frac{\int x^3 dx \mathcal{Y}^{(n)}}{\int x^3 dx \mathcal{Y}^{(0)}} = \frac{\int x^3 dx \mathcal{G}^{(n)}}{\int x^3 dx \mathcal{G}^{(0)}} = \frac{I_n}{I_0}. \quad (71)$$

Assuming standard power law initial power spectrum

$$\mathcal{P}_\zeta = A_\zeta \left(\frac{k}{k_0} \right)^{n_s-1}, \quad (72)$$

with $k_0 \text{Mpc}/h = 0.05$ and $n_s = 0.96$, we integrate the Fourier momentum in Eq. (64) and find

$$\langle y_0^{(4)} \rangle = \int_z^\infty d \ln(1+z) \left(\mathcal{S}^{(0,4)} + \mathcal{S}^{(4,0)} \right), \quad (73)$$

where

$$\mathcal{S}^{(X)}(z) \equiv \int_{k_{\min}}^{k_{\max}} d \ln k \mathcal{P}_\zeta \mathcal{J}_y \frac{\mathcal{K}^{(X)}}{H}. \quad (74)$$

The source functions $\mathcal{S}^{(X)}$ in units of A_ζ as a function of the redshift are shown in the right panel of Fig. 2.

D. Acoustic dissipation

Rayleigh scattering is an additional photon scattering that makes photon-baryon coupling stronger. Hence, Rayleigh scattering decreases the multipole anisotropy during the tight coupling regime. As a result, the energy released from acoustic oscillation is reduced. Thus, the new spectral distortion is a negative contribution to the y distortion during the tight coupling regime. Combining Eqs. (34), (35), (36) and (66), we find

$$\langle y_0^{(4)} \rangle' \sim -\frac{\dot{\tau}^{(4)}}{\dot{\tau}^{(0)}} \langle y_0^{(0)} \rangle', \quad (75)$$

which is consistent with both panels in Fig. 2. Including Rayleigh scattering effectively implies increasing baryons for Thomson scattering, and we also confirmed $\partial y^{(0)}/\partial \Omega_b < 0$ during recombination.

After hydrogen recombination, Thomson scattering is less efficient. Then, Rayleigh scattering adds extra diffusion, which causes a positive spectral distortion. Energy contribution from the final recombination stage is dominant because hydrogen Rayleigh scattering is most significant. For $n_s = 0.96$ and $A_\zeta = 2.196 \times 10^{-9}$, the main contribution comes from $k \text{Mpc}/h \sim 0.1$, and the total new spectral distortion has the same sign as y . We found a new spectral distortion from acoustic dissipation during recombination is $y_{\text{ac}}^{(4)} \mathcal{J}^{(4)} = 4 \times 10^{-3} \text{Jy/str}$ around $\nu = 300 \text{GHz}$ and 600GHz in Fig. 4. We also confirmed that the y distortion decreases by 0.1%, including the backreaction effect. Those corrections are one order of magnitude smaller than the sensitivity range of ESA voyage 2050 [8, 9].

E. Reionization

After hydrogen recombination, both Thomson scattering and Rayleigh scattering are inefficient. Photons free-

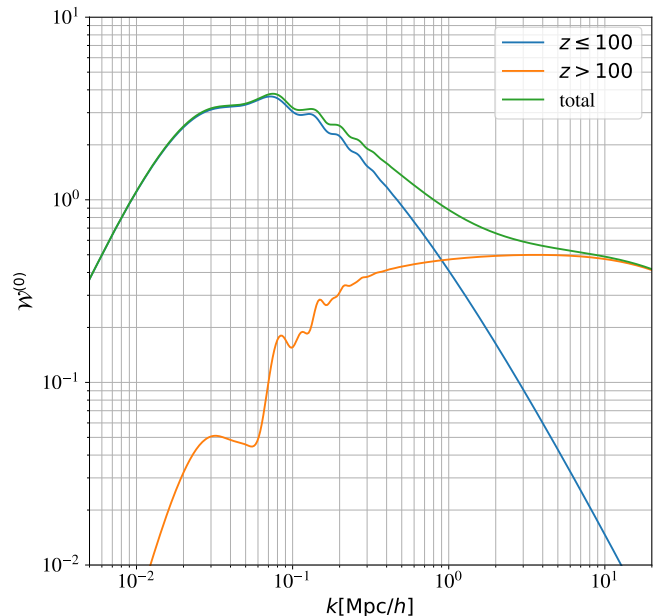


FIG. 3. The y distortion window functions for $z \leq 100$ and $z > 100$. The window function for $z \leq 100$ is amplified because the baryon velocity is growing with the dark matter sector. Such a reionization enhancement does not happen for Rayleigh scattering.

stream while baryons evolve like dark matter after recombination. Reionization introduces additional y spectral distortion since the source term is enhanced drastically as $V_1 \gg \Theta_1^{(0)}$ at a late time. y distortion from the reionization is five times bigger than recombination. The Fourier space window functions for $z \leq 100$ and $z > 100$ are shown in Fig. 3. Including reionization contribution $y_{\text{reio}}^{(0)} = 2.4 \times 10^{-8}$, we find the total spectral distortion $y^{(0)} = 2.9 \times 10^{-8}$ at present. Rayleigh scattering will not happen at a late time since the photon energy is too small; therefore, $\mathcal{S}^{(4,0)}$ is negligible for reionization. The Rayleigh anisotropies produced during recombination can also be Thomson scattered after reionization. However, the Rayleigh dipole $\Theta_1^{(4)}$ is not enhanced, unlike $\Theta_{1g}^{(0)}$ since it does not have the baryon velocity. Hence, $\mathcal{S}^{(0,4)}$ is also negligible. We evaluated the spectral distortion from Rayleigh scattering after reionization, and we found that it is 0.1% of the recombination one. Thus, Rayleigh scattering will not generate secondary spectral distortions during reionization.

F. Compton cooling

So far, we have ignored the relativistic correction T_e/m_e to the Boltzmann equation. This term leads to the relativistic correction to the isotropic part of the photon distribution function independently from second-order perturbations. The relativistic correction to the

Thomson scattering collision integral is (see e.g., [36] for a derivation)

$$-\dot{\tau}^{(0)} \frac{T_e}{m_e} \left(x^2 \frac{\partial^2}{\partial x^2} + 4x \frac{\partial}{\partial x} \right) f - \dot{\tau}^{(0)} \frac{T_{\text{CMB}}(1+z)}{m_e} \left[x^2 \frac{\partial}{\partial x} + 4x \right] f(1+f), \quad (76)$$

and for $f = f_{\text{pl}}$, Eq. (76) turns into

$$-\dot{\tau}^{(0)} \left[\frac{T_e}{m_e} - \frac{T_{\text{CMB}}(1+z)}{m_e} \right] \mathcal{Y}^{(0)}. \quad (77)$$

The y distortion from this term is called Compton cooling as the electron temperature is always slightly lower than the photon's, and photons are cooled via Compton scattering [21]. Including reionization, we found $y_e^{(0)} = 2.74 \times 10^{-10}$, which is subdominant to acoustic dissipation. With the same prescription as Sec. IV A, we found $\mathcal{Y}^{(0)}$ is replaced with $\mathcal{Y}^{(4)}$ for Rayleigh scattering and find the following additional contribution

$$-\dot{\tau}^{(4)} \left[\frac{T_e}{m_e} - \frac{T_{\text{CMB}}(1+z)}{m_e} \right] \mathcal{Y}^{(4)}. \quad (78)$$

Since $\tau^{(4)}$ is suppressed during reionization, the Compton cooling via Rayleigh scattering only happens during recombination. The cooling effect for Rayleigh scattering is estimated as $y_e^{(4)} \mathcal{Y}^{(4)} \sim 2.5 \times 10^{-3} \text{ Jy/str}$. As Rayleigh scattering introduces an additional cooling effect, the spectral distortion has the same sign as the standard cooling effect. $y_{\text{ac}}^{(0)}$ is sourced during recombination, but $y_e^{(0)}$ is produced only at the end of recombination. As a result, we find $y_e^{(0)} \ll y_{\text{ac}}^{(0)}$. On the other hand, both $y_{\text{ac}}^{(4)}$ and $y_e^{(4)}$ are sourced at the end of recombination; those signals are comparable. The total $y^{(4)}$ increases by about 60% after including the cooling effect.

G. Sunyaev-Zel'dovich effect

y spectral distortion from recombination is useful observable for tests of primordial perturbations at $0.1 \leq k\text{Mpc}/h \leq 100$ [11, 12]. However, $\mathcal{Y}^{(0)}$ -type spectral dependence is dominated by the thermal Sunyaev-Zel'dovich effect, i.e., the Compton scattering between the CMB photons and hot electron gas in the late Universe. The typical size of $y_{\text{tSZ}}^{(0)}$ is 10^{-6} [48], which is 100 times bigger than the primordial signals even after including reionization enhancement. The tSZ effect is indistinguishable from reionization or recombination signals. The degeneration is a crucial disadvantage of y spectral distortion for primordial perturbation search. While the new spectral distortion from Rayleigh scattering is weak, Rayleigh scattering must not secondarily produce the signal after recombination because the photons must be sufficiently hot. For clusters at $z < 10$,

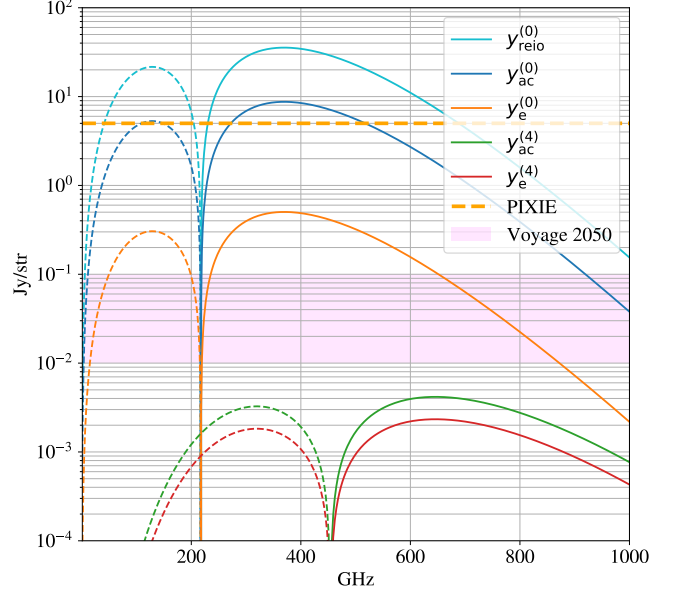


FIG. 4. The y spectral distortion and the new spectral distortion from Rayleigh scattering with future experimental target sensitivities. The spectral distortions are evaluated for cosmological parameters consistent with the recent CMB anisotropy measurements.

the suppression factor is below 10^{-8} . Therefore, the new spectral distortions are straightforwardly related to cosmology during recombination.

V. CONSTRAINTS ON COSMOLOGY

We calculated the new spectral distortions for the standard power-law initial spectrum and found the total spectral distortion, including the cooling effect, is $6.5 \times 10^{-3} \text{ Jy/str}$. The size is about 0.7% of the y spectral distortion from recombination and one order of magnitude smaller than the target sensitivity range of voyage 2050 [8, 9]. Observing the new spectral distortions for the standard cosmological scenario with the almost scale invariant curvature perturbations is quite difficult. However, there are a few advantages of the new spectral distortions. The y spectral distortion degenerates with the tSZ effect, which is 10^3 times bigger than the y distortion from recombination. Therefore, we cannot use $y^{(0)}$ for cosmological constraints about recombination even if the sensitivity goes beyond 10^{-3} Jy/str . The new spectral distortion is free from the issue. We can extract the cosmological information from ideal measurements of $y^{(4)}$ and crosscheck cosmology determined by other surveys such as Planck [44].

There are two peaks in the right panel of Fig. 2. The first negative peak around $z \sim 6000$ is due to Rayleigh scattering of singly ionized helium during the tight-coupling regime. The second positive peak is from neutral hydrogen Rayleigh scattering. The late time

peak dominates the total distortion for the almost scale-invariant power spectrum because hydrogen Rayleigh scattering is more efficient than singly ionized helium.

The scale dependence of the sign could be potentially useful to distinguish several nonstandard scenarios. For example, let us consider a blue tilted initial spectrum, i.e., $n_s > 1$. As we have $\log_{10}[W^{(0,4)}(k\text{Mpc}/h = 1.)/\mathcal{W}^{(4,0)}(k\text{Mpc}/h = 0.1)] \approx 3.4$, the negative part dominates for the blue spectrum with $n_s \gtrsim 4.4$. However, such a highly blue spectrum also introduces detectable spectral distortions like μ spectral distortions [49]. Several inflationary models predict peaks in the curvature power spectrum that can be approximated by the log-normal spectrum

$$\mathcal{P}_\zeta = \frac{A_\zeta}{\sqrt{2\pi}\Delta} e^{-\frac{(\ln k - \ln k_0)^2}{2\Delta^2}}, \quad (79)$$

which is often considered for primordial black hole formation and associated induced gravitational waves [50]. Consider the peak located at $k_0\text{Mpc}/h = 2.$, with $A_\zeta = 10^{-4}$ and $\Delta = 10^{-3}$. We cannot exclude such a lognormal spectrum from the current temperature anisotropy measurements since the CMB anisotropies at $k\text{Mpc}/h > 0.1$ is exponentially suppressed due to Silk damping. In this setup, we find $y_{\text{ac}}^{(0)} = 1. \times 10^{-6}$, which is comparable to the tSZ effect, so we cannot distinguish the tSZ effect from $y_{\text{ac}}^{(0)}$. For the same parameters, we find the new spectral distortion is $3. \times 10^{-2}\text{Jy/str}$ with the opposite sign, which is in the target range of voyage 2050.

VI. CONCLUSIONS

Towards future precise CMB intensity spectral measurements [5–9], we considered a new spectral distortion from Rayleigh scattering during recombination. There are a few works on the Rayleigh anisotropies [28–32], but all of them are about the linear anisotropies, and thus distortions to the angular averaged spectrum have not been considered. In this work, we expanded the photon Boltzmann equation to second-order cosmological perturbations in the presence of Thomson scattering and Rayleigh scattering, and we show that the second-order effect introduces a new monopole spectral distortion. The generation mechanism is similar to the traditional y spectral distortion from the relativistic corrections to the Thomson scattering. We show that Rayleigh scattering also introduces the frequency-dependent acoustic dissipation and Compton cooling effect. The spectral shape is different from the other traditional spectral distortions. Spectral distortions from atomic processes during recombination were studied at the background level in the literature, but those works do not include Rayleigh scattering

since diffusion introduced by second order perturbations is mandatory for the present consideration [16–19].

Fig. 4 shows several y and new spectral distortions obtained in this work. We found the new spectral distortion, including both acoustic dissipation and the cooling effect, is $6.5 \times 10^{-3}\text{Jy/str}$ for the cosmological parameters determined by Ref. [44], which is one order of magnitude smaller than the envisioned target sensitivity range of voyage 2050. Thus, the spectral distortion from the second-order Rayleigh scattering is tiny, and it will not be easy to detect the signal soon.

Even if the new spectral distortion is tiny, it can be useful. The scale invariant primordial density perturbations at $0.01 \leq k\text{Mpc} \leq 100$ yields $y \sim 10^{-9}$, which is the detectable size in the next generation of spectral measurements. However, the Sunyaev-Zel’dovich effect is known as the same spectral dependence as the y distortion; Compton scattering of the CMB photons by high energy electron gas in the late time clusters is three orders of magnitude bigger than the primordial y distortion. In principle, the sky averages degenerate. The new spectral distortion is not produced in the late Universe because CMB photons are too cold for Rayleigh scattering after recombination. In the longer term, the new spectral distortion can be distinguishable from other signals and can be more useful than the traditional y distortion for recombination studies. We also considered several scale-dependent primordial power spectra for the new spectral distortion, and we showed that there is a unique window for constraining the large initial perturbations at $k\text{Mpc}/h \sim 1$.

Rayleigh scattering adds new electrons interacting with photons; therefore, the photon-electron coupling becomes stronger. As a result, the multipole anisotropies are suppressed, and then the acoustic dissipation is reduced during the tight coupling regime. Thus, additional interacting species suppress the acoustic source in the early Universe. Such a response will be universal; therefore, spectral distortions will be useful for constraining unknown interacting dark sectors.

We considered a rigorous framework of second-order Boltzmann equations for isotropic spectral distortions. Full second-order CMB, including Rayleigh scattering, will be more complicated but important to subtract the intrinsic nonlinearity for constraining the primordial non-Gaussianity in the Rayleigh anisotropies. The extension to the full second-order CMB will be discussed elsewhere.

ACKNOWLEDGMENTS

The author would like to thank William R. Coulton for his useful discussions.

- Astrophys. Space Sci.*, 4:301–316, 1969. doi:10.1007/BF00661821.
- [2] R. A. Sunyaev and Ya. B. Zeldovich. Small scale fluctuations of relic radiation. *Astrophys. Space Sci.*, 7:3–19, 1970.
 - [3] Wayne Hu and Joseph Silk. Thermalization and Spectral Distortions of the Cosmic Background Radiation. *Phys. Rev.*, D48:485–502, 1993. doi:10.1103/PhysRevD.48.485.
 - [4] D. J. Fixsen, E. S. Cheng, J. M. Gales, John C. Mather, R. A. Shafer, and E. L. Wright. The Cosmic Microwave Background Spectrum from the Full Cobe Firas Data Set. *Astrophys. J.*, 473:576, 1996. arXiv:astro-ph/9605054, doi:10.1086/178173.
 - [5] A. Kogut et al. The Primordial Inflation Explorer (Pixie): a Nulling Polarimeter for Cosmic Microwave Background Observations. *JCAP*, 1107:025, 2011. arXiv:1105.2044, doi:10.1088/1475-7516/2011/07/025.
 - [6] A. Kogut, M. H. Abitbol, J. Chluba, J. Delabrouille, D. Fixsen, J. C. Hill, S. P. Patil, and A. Rotti. Cmb Spectral Distortions: Status and Prospects. 7 2019. arXiv:1907.13195.
 - [7] Philippe André et al. PRISM (Polarized Radiation Imaging and Spectroscopy Mission): An Extended White Paper. *JCAP*, 02:006, 2014. arXiv:1310.1554, doi:10.1088/1475-7516/2014/02/006.
 - [8] J. Chluba et al. Spectral Distortions of the Cmb as a Probe of Inflation, Recombination, Structure Formation and Particle Physics: Astro2020 Science White Paper. *Bull. Am. Astron. Soc.*, 51(3):184, 2019. arXiv:1903.04218.
 - [9] J. Chluba et al. New Horizons in Cosmology with Spectral Distortions of the Cosmic Microwave Background. *Exper. Astron.*, 51(3):1515–1554, 2021. arXiv:1909.01593, doi:10.1007/s10686-021-09729-5.
 - [10] Wayne Hu, Douglas Scott, and Joseph Silk. Power Spectrum Constraints from Spectral Distortions in the Cosmic Microwave Background. *Astrophys. J.*, 430:L5–L8, 1994. arXiv:astro-ph/9402045, doi:10.1086/187424.
 - [11] Jens Chluba, Rishi Khatri, and Rashid A. Sunyaev. Cmb at 2X2 Order: the Dissipation of Primordial Acoustic Waves and the Observable Part of the Associated Energy Release. *Mon. Not. Roy. Astron. Soc.*, 425:1129–1169, 2012. arXiv:1202.0057, doi:10.1111/j.1365-2966.2012.21474.x.
 - [12] Jens Chluba, Adrienne L. Erickcek, and Ido Ben-Dayan. Probing the Inflaton: Small-Scale Power Spectrum Constraints from Measurements of the Cmb Energy Spectrum. *Astrophys. J.*, 758:76, 2012. arXiv:1203.2681, doi:10.1088/0004-637X/758/2/76.
 - [13] James B. Dent, Damien A. Easson, and Hiroyuki Tashiro. Cosmological Constraints from Cmb Distortion. *Phys. Rev. D*, 86:023514, 2012. arXiv:1202.6066, doi:10.1103/PhysRevD.86.023514.
 - [14] Atsuhisa Ota, Tomo Takahashi, Hiroyuki Tashiro, and Masahide Yamaguchi. CMB μ distortion from primordial gravitational waves. *JCAP*, 10:029, 2014. arXiv:1406.0451, doi:10.1088/1475-7516/2014/10/029.
 - [15] Atsuhisa Ota and Nicola Bartolo. Cmb Spectroscopy at Third-Order in Cosmological Perturbations. *Phys. Rev.*, D100(4):043521, 2019. arXiv:1808.10517, doi:10.1103/PhysRevD.100.043521.
 - [16] Wan Yan Wong, Sara Seager, and Douglas Scott. Spectral Distortions to the Cosmic Microwave Background from the Recombination of Hydrogen and Helium. *Mon. Not. Roy. Astron. Soc.*, 367:1666–1676, 2006. arXiv:astro-ph/0510634, doi:10.1111/j.1365-2966.2006.10076.x.
 - [17] R. A. Sunyaev and J. Chluba. Signals from the Epoch of Cosmological Recombination. *Astron. Nachr.*, 330:657–674, 2009. arXiv:0908.0435, doi:10.1002/asna.200911237.
 - [18] Jens Chluba and Yacine Ali-Haïmoud. Cosmospes: Fast and Detailed Computation of the Cosmological Recombination Radiation from Hydrogen and Helium. *Mon. Not. Roy. Astron. Soc.*, 456(4):3494–3508, 2016. arXiv:1510.03877, doi:10.1093/mnras/stv2691.
 - [19] J. Chluba and R. A. Sunyaev. Pre-Recombinational Energy Release and Narrow Features in the Cmb Spectrum. *Astron. Astrophys.*, 501:29–47, 2009. arXiv:0803.3584, doi:10.1051/0004-6361/200809840.
 - [20] J. Chluba. Could the Cosmological Recombination Spectrum Help Us Understand Annihilating Dark Matter? *Mon. Not. Roy. Astron. Soc.*, 402:1195, 2010. arXiv:0910.3663, doi:10.1111/j.1365-2966.2009.15957.x.
 - [21] J. Chluba and R. A. Sunyaev. The Evolution of Cmb Spectral Distortions in the Early Universe. *Mon. Not. Roy. Astron. Soc.*, 419:1294–1314, 2012. arXiv:1109.6552, doi:10.1111/j.1365-2966.2011.19786.x.
 - [22] Jens Chluba and Donghui Jeong. Teasing Bits of Information Out of the Cmb Energy Spectrum. *Mon. Not. Roy. Astron. Soc.*, 438(3):2065–2082, 2014. arXiv:1306.5751, doi:10.1093/mnras/stt2327.
 - [23] Tracy R. Slatyer. Indirect Dark Matter Signatures in the Cosmic Dark Ages II. Ionization, Heating and Photon Production from Arbitrary Energy Injections. *Phys. Rev. D*, 93(2):023521, 2016. arXiv:1506.03812, doi:10.1103/PhysRevD.93.023521.
 - [24] Yacine Ali-Haïmoud. Testing dark matter interactions with CMB spectral distortions. *Phys. Rev. D*, 103(4):043541, 2021. arXiv:2101.04070, doi:10.1103/PhysRevD.103.043541.
 - [25] Saurabh Kumar, Emanuela Dimastrogiovanni, Glenn D. Starkman, Craig Copi, and Bryan Lynn. Cmb Spectral Distortions from Cooling Macroscopic Dark Matter. *Phys. Rev. D*, 99(2):023521, 2019. arXiv:1804.08601, doi:10.1103/PhysRevD.99.023521.
 - [26] Sandeep Kumar Acharya and Rishi Khatri. New Cmb Spectral Distortion Constraints on Decaying Dark Matter with Full Evolution of Electromagnetic Cascades Before Recombination. *Phys. Rev. D*, 99(12):123510, 2019. arXiv:1903.04503, doi:10.1103/PhysRevD.99.123510.
 - [27] Ki-Young Choi, Kenji Kadota, and Inwoo Park. Constraining Dark Photon Model with Dark Matter from Cmb Spectral Distortions. *Phys. Lett. B*, 771:162–167, 2017. arXiv:1701.01221, doi:10.1016/j.physletb.2017.04.062.
 - [28] Qing-Juan Yu, David N. Spergel, and Jeremiah P. Ostriker. Rayleigh Scattering and Microwave Background Fluctuations. *Astrophys. J.*, 558:23–28, 2001. arXiv:astro-ph/0103149, doi:10.1086/322482.
 - [29] Antony Lewis. Rayleigh Scattering: Blue Sky Thinking for Future Cmb Observations. *JCAP*, 1308:053, 2013. arXiv:1307.8148, doi:10.1088/1475-7516/2013/08/053.
 - [30] Elham Alipour, Kris Sigurdson, and Christopher M. Hirata. Effects of Rayleigh Scattering on the Cmb and Cosmic Structure. *Phys. Rev.*, D91(8):083520, 2015.

- arXiv:1410.6484, doi:10.1103/PhysRevD.91.083520.
- [31] Benjamin Beringue, P. Daniel Meerburg, Joel Meyers, and Nicholas Battaglia. Cosmology with Rayleigh Scattering of the Cosmic Microwave Background. *JCAP*, 01:060, 2021. arXiv:2008.11688, doi:10.1088/1475-7516/2021/01/060.
 - [32] William R. Coulton, Benjamin Beringue, and P. Daniel Meerburg. Primordial information content of Rayleigh anisotropies. *Phys. Rev. D*, 103(4):043501, 2021. arXiv:2010.10481, doi:10.1103/PhysRevD.103.043501.
 - [33] Cyril Pitrou, Francis Bernardeau, and Jean-Philippe Uzan. The Y-Sky: Diffuse Spectral Distortions of the Cosmic Microwave Background. *JCAP*, 1007:019, 2010. arXiv:0912.3655, doi:10.1088/1475-7516/2010/07/019.
 - [34] Sébastien Renaux-Petel, Christian Fidler, Cyril Pitrou, and Guido W. Pettinari. Spectral distortions in the cosmic microwave background polarization. *JCAP*, 03:033, 2014. arXiv:1312.4448, doi:10.1088/1475-7516/2014/03/033.
 - [35] Cyril Pitrou and Albert Stebbins. Parameterization of Temperature and Spectral Distortions in Future Cmb Experiments. *Gen. Rel. Grav.*, 46(11):1806, 2014. arXiv:1402.0968, doi:10.1007/s10714-014-1806-z.
 - [36] Atsuhisa Ota. Cmb Spectral Distortions as Solutions to the Boltzmann Equations. *JCAP*, 1701(01):037, 2017. arXiv:1611.08058, doi:10.1088/1475-7516/2017/01/037.
 - [37] Cyril Pitrou. Radiative Transport of Relativistic Species in Cosmology. *Astropart. Phys.*, 125:102494, 2021. arXiv:1902.09456, doi:10.1016/j.astropartphys.2020.102494.
 - [38] J. Fisak, J. Krticka, D. Munzar, and J. Kubat. Rayleigh scattering in the atmospheres of hot stars. *Astronomy & Astrophysics*, 590:A95, May 2016. URL: <http://dx.doi.org/10.1051/0004-6361/201628291>, doi:10.1051/0004-6361/201628291.
 - [39] Sara Seager, Dimitar D. Sasselov, and Douglas Scott. A New Calculation of the Recombination Epoch. *Astrophys. J. Lett.*, 523:L1–L5, 1999. arXiv:astro-ph/9909275, doi:10.1086/312250.
 - [40] Yacine Ali-Haïmoud and Christopher M. Hirata. Hyrec: a Fast and Highly Accurate Primordial Hydrogen and Helium Recombination Code. *Phys. Rev. D*, 83:043513, 2011. arXiv:1011.3758, doi:10.1103/PhysRevD.83.043513.
 - [41] Scott Dodelson. *Modern Cosmology*. Academic Press, Amsterdam, 2003.
 - [42] Chung-Pei Ma and Edmund Bertschinger. Cosmological Perturbation Theory in the Synchronous and Conformal Newtonian Gauges. *Astrophys. J.*, 455:7–25, 1995. arXiv:astro-ph/9506072, doi:10.1086/176550.
 - [43] Diego Blas, Julien Lesgourgues, and Thomas Tram. The Cosmic Linear Anisotropy Solving System (CLASS) II: Approximation Schemes. *JCAP*, 1107:034, 2011. arXiv:1104.2933, doi:10.1088/1475-7516/2011/07/034.
 - [44] N. Aghanim et al. Planck 2018 Results. VI. Cosmological Parameters. *Astron. Astrophys.*, 641:A6, 2020. arXiv:1807.06209, doi:10.1051/0004-6361/201833910.
 - [45] Atsuhisa Ota and Masahide Yamaguchi. Secondary Isocurvature Perturbations from Acoustic Reheating. *JCAP*, 1806(06):022, 2018. arXiv:1705.05196, doi:10.1088/1475-7516/2018/06/022.
 - [46] René D. Rohrmann. Rayleigh scattering in dense fluid helium. *MNRAS*, 473(1):457–469, January 2018. arXiv:1709.07076, doi:10.1093/mnras/stx2440.
 - [47] Jens Chluba. Green’s Function of the Cosmological Thermalization Problem. *Mon. Not. Roy. Astron. Soc.*, 434:352, 2013. arXiv:1304.6120, doi:10.1093/mnras/stt1025.
 - [48] Alexandre Refregier, Eiichiro Komatsu, David N. Spergel, and Ue-Li Pen. Power Spectrum of the Sunyaev-Zel’dovich Effect. *Phys. Rev. D*, 61:123001, 2000. arXiv:astro-ph/9912180, doi:10.1103/PhysRevD.61.123001.
 - [49] Giovanni Cabass, Alessandro Melchiorri, and Enrico Pajer. μ distortions or running: A guaranteed discovery from CMB spectrometry. *Phys. Rev. D*, 93(8):083515, 2016. arXiv:1602.05578, doi:10.1103/PhysRevD.93.083515.
 - [50] Shi Pi and Misao Sasaki. Gravitational Waves Induced by Scalar Perturbations with a Lognormal Peak. *JCAP*, 09:037, 2020. arXiv:2005.12306, doi:10.1088/1475-7516/2020/09/037.